J. Math. Anal. Appl. 449 (2017) 1601–1618

Contents lists available at ScienceDirect

Journal of Mathematical Analysis and Applications

www.elsevier.com/locate/jmaa

Admittivity imaging from multi-frequency micro-electrical impedance tomography ☆

Habib Ammari [a,*], Laure Giovangigli [b], Loc Hoang Nguyen [c], Jin-Keun Seo [d]

[a] *Department of Mathematics, ETH Zürich, Rämistrasse 101, CH-8092 Zürich, Switzerland*
[b] *Department of Mathematics, 340 Rowland Hall, University of California at Irvine, Irvine, CA 92697-3875, USA*
[c] *Department of Mathematics & Statistics, University of North Carolina, Charlotte, Charlotte, NC 28223, USA*
[d] *Department of Computational Science and Engineering, Yonsei University, 50 Yonsei-Ro, Seodaemun-Gu, Seoul 120-749, Republic of Korea*

ARTICLE INFO

Article history:
Received 21 July 2014
Available online 6 January 2017
Submitted by H. Kang

Keywords:
Imaging from internal data
Micro-electrical impedance tomography
Multi-frequency measurements
Optimal control
Landweber algorithm

ABSTRACT

The aim of this paper is to propose an optimal control optimization algorithm for reconstructing admittivity distributions (i.e., both conductivity and permittivity) from multi-frequency micro-electrical impedance tomography. A convergent and stable optimal control scheme is shown to be obtainable from multi-frequency data. This opens a door for convergence analysis of optimal control type approaches in imaging from internal data. The results of this paper have potential applicability in cancer imaging, cell culturing and differentiation, food sciences, and biotechnology.

1. Introduction

This paper aims at proposing and analyzing an optimal control approach for imaging the admittivity distributions of biological tissues. To the best of our knowledge, it provides for the first time a convergence proof of an optimal control approach for reconstructing parameter distributions from internal data.

Biological tissues possess characteristic distributions of permittivity and conductivity [41]. Conductivity can be regarded as a measure of the ability to transport charge throughout material's volume under an applied electric field, while permittivity is a measure of the ability of the dipoles within a material to rotate (or of the material to store charge) under an applied external field. At low frequencies, biological tissues behave like a conductor, but capacitive effects become important at higher frequencies due to the

☆ This work was supported by the ERC Advanced Grant Project MULTIMOD-267184.
* Corresponding author.
E-mail addresses: habib.ammari@math.ethz.ch (H. Ammari), lgiovang@uci.edu (L. Giovangigli), nguye50@uncc.edu (L.H. Nguyen), seoj@yonsei.ac.kr (J.-K. Seo).

http://dx.doi.org/10.1016/j.jmaa.2017.01.004
0022-247X/

membranous structures [46,40,48]. The electric behavior of a biological tissue under the influence of an electric field at frequency ω can be characterized by its frequency-dependent admittivity $\sigma + i\omega\varepsilon$, where σ and ε are respectively its conductivity and permittivity. As recently shown in [13,48], spectroscopic admittivity imaging can provide information about the microscopic structure of a medium, from which physiological or pathological conditions of tissue can be derived, because the admittivity of biological tissue varies with its composition, membrane characteristics, intra-and extra-cellular fluids, and other factors.

In this paper, we consider the imaging of admittivity distributions of biological tissues from multi-frequency micro-electrical impedance data. Micro-electrical impedance tomography [34,38,25,42] can be used to reconstruct a high resolution admittivity distribution from internal measurements of electrical potential at multiple frequencies. The technique uses planar arrays of micro-electrodes to nondestructively sense thin layers of biological samples [20,34,35,44,52]. It has potential applications in cell electrofusion and electroporation, cell culturing, cell differentiation and drug screening; see [18,34,36,37,39,42,30,43,45,54]. It is capable of high-resolution imaging. Other methods of electrical tissue property imaging using internal data are investigated in [9–12,17,24,49,50,53]. Resolution and stability enhancements are achieved from internal measurements [14–16].

To solve the admittivity imaging problem from multi-frequency micro-electrical data, we propose an optimal control optimization algorithm and rigorously prove its stability and convergence properties. Internal potential measurements at a single frequency may be insufficient for reconstructing the admittivity distribution. An initial guess is constructed by solving a boundary value problem. Note that the method of characteristics [32] can not be used to solve the transport equation satisfied by the logarithm of the admittivity, because the electrical potential is a complex valued function. It is unlikely that a direct (noniterative) method can be designed for solving the admittivity imaging problem. As far as we know, the approach in this paper and the analysis of its convergence and stability have not been reported elsewhere. Moreover, the convergence of the optimal control approach is the first convergence result for reconstruction algorithms from internal data.

To formulate mathematically the imaging problem, we consider a medium of conductivity σ and permittivity ε occupying Ω, $\mathcal{C}^2$-domain of $\mathbb{R}^2$. (Hereafter, the medium is simply called Ω.) The problem of micro-electrical impedance tomography is to reconstruct σ and ε from the vector of potential u_ω, $\omega \in (\underline{\omega}, \overline{\omega})$, the solution of

$$\begin{cases} \nabla \cdot (\sigma + i\omega\varepsilon)\nabla u_\omega = 0 \ \text{ in } \Omega, \\ u_\omega = \varphi \ \text{ on } \partial\Omega, \end{cases} \tag{1.1}$$

where $\varphi = (\varphi_1, \varphi_2) \in H^{1/2}(\partial\Omega)^2$. It is proved in this paper that the above inverse problem is stably solvable with a good choice of boundary datum φ; that is, φ belongs to what we will refer to as the proper set of boundary measurements; see [11,49,51].

It is worth noticing that in the case $\omega = 0$, it is possible to construct a priori suitable boundary conditions such that the Jacobian of two solutions of (1.1) never cancels. This follows from some generalizations of the Rado–Kneser–Choquet theorem (see [19,7,8]). The proof of this result heavily relies on the fact that the space dimension is two and on the maximum principle. In three dimensions, this result is known to be false [21,22]. Since the maximum principle plays a key role in the argument, and it does not hold for our PDE if $\omega > 0$ ([31, Chapter 2]), it is expected that if $\omega > 0$ we cannot find a priori boundary conditions guaranteeing a non-zero Jacobian everywhere. Even though there are valid theoretical reasons to believe that this is the case, as far as the authors are aware this hasn't been considered before. It should also be pointed out that as in [22] the counter-example may not be so obvious to construct. On the other hand, the use of multiple frequencies has shown to be effective to overcome this type of issue (when everything is fine for $\omega = 0$ but you are interested in the case $\omega > 0$), see [1–5], and this is what we carry on in this paper. We prove convergence of an optimal control method by using multiple frequencies.

The paper is organized as follows. First, in section 2 we review some useful regularity results for elliptic systems of partial differential equations. In section 3 we introduce the set of proper boundary measurements. Section 4 is devoted to the reconstruction method. We prove that the minimization functional is Fréchet differentiable and compute its derivative. Then we construct an initial guess and prove the convergence of a minimizing sequence. Some numerical examples that support our findings are provided in section 5. The paper ends with a short discussion. In the appendix, we prove the convergence of Landweber sequences with cutoff functions.

2. Preliminaries on regularities

Let $\Omega' = \{x \in \Omega \ : \ \mathrm{dist}(x, \partial\Omega) > c_0\}$ for a small constant $c_0 > 0$. We assume that σ and ε are constant and known in $\Omega \setminus \Omega'$. In the following, we let σ_* and ε_*, the true conductivity and permittivity of Ω, belong to the convex subset of $H^2(\Omega)^2$ given by

$$\widetilde{\mathcal{S}} = \{(\sigma, \varepsilon) := (\sigma_0, \varepsilon_0) + (\eta_1, \eta_2) | \, (\eta_1, \eta_2) \in \mathcal{S}\},$$

where the positive constants σ_0 and ε_0 are respectively the conductivity and permittivity in $\Omega \setminus \Omega'$ and

$$\begin{aligned} \mathcal{S} = \{(\eta_1, \eta_2) \in H_0^2(\Omega)^2 | \ & c_1 < \eta_1 + \sigma_0 < c_2, \ c_1 < \eta_2 + \epsilon_0 < c_2, \ \mathrm{supp}\ \eta_j \subset \Omega', \\ & \|\eta_j\|_{H^2(\Omega)} \le c_3 \|\eta_j\|_{H^1(\Omega)}, \ \|\eta_j\|_{H^1(\Omega)} \le c_4 \ \text{ for } j = 1, 2 \ \} \end{aligned} \tag{2.1}$$

with c_1, c_2, c_4 and c_4 being positive constants and supp denoting the support. In other words, we can write $\widetilde{\mathcal{S}} = (\sigma_0, \varepsilon_0) + \mathcal{S}$. Here, the condition of

$$\|\eta_j\|_{H^2(\Omega)} \le c_3 \|\eta_j\|_{H^1(\Omega)}$$

is used to exclude any micro-local oscillation on the admittivity distribution.

Introducing an open subset of $\mathbb{C}$

$$\mathcal{O} := \left\{ o \in \mathbb{C} | \Im m\, o < \frac{c_1}{2c_2} \right\}, \tag{2.2}$$

we first establish a useful lemma, which is a direct consequence of standard regularity results [23,26,27].

Lemma 2.1. *Let $(\sigma, \varepsilon) \in \widetilde{\mathcal{S}}$, $\omega \in \mathcal{O}$, and $f \in L^p(\Omega)$ for $2 \le p < \infty$. If $v \in H^1(\Omega)$ satisfy*

$$\nabla \cdot (\sigma + i\omega\varepsilon)\nabla v = f \quad \text{in} \quad \Omega, \tag{2.3}$$

then $v \in W^{2,p}(\Omega')$ and

$$\|v\|_{W^{2,p}(\Omega')} \ \le \ C \ (\|v\|_{L^p(\Omega)} + \|f\|_{L^p(\Omega)}), \tag{2.4}$$

where C depends only on $c_i, i = 0, \ldots, 4$, p, and Ω. Moreover, if $v = 0$ on $\partial\Omega$, then

$$\|v\|_{W^{2,p}(\Omega)} \ \le \ C \ (\|v\|_{L^p(\Omega)} + \|f\|_{L^p(\Omega)}). \tag{2.5}$$

Proof. From the standard regularity estimate, we have

$$\|v\|_{H^2(\Omega')} \ \le \ C \ (\|f\|_{L^2(\Omega)^2} + \|v\|_{L^2(\Omega)}). \tag{2.6}$$

The first equation in (1.1) can be rewritten as

$$\Delta v = -\nabla v^T \frac{\nabla(\sigma + i\omega\varepsilon)}{\sigma + i\omega\varepsilon} + \frac{f}{\sigma + i\omega\varepsilon}, \tag{2.7}$$

where T denotes the transpose. Since supp $\nabla(\sigma + i\omega\varepsilon) \subset \Omega'$, we have

$$\begin{aligned}
\|\nabla v^T \frac{\nabla(\sigma + i\omega\varepsilon)}{\sigma + i\omega\varepsilon}\|_{L^p(\Omega)} &= \|\nabla v^T \frac{\nabla(\sigma + i\omega\varepsilon)}{\sigma + i\omega\varepsilon}\|_{L^p(\Omega')} \\
&\leq C\|\nabla v^T\|_{L^{2p}(\Omega')^2} \|\frac{\nabla(\sigma + i\omega\varepsilon)}{\sigma + i\omega\varepsilon}\|_{L^{2p}(\Omega')^2} \\
&\leq C\|v\|_{H^2(\Omega')}\|\sigma + i\omega\varepsilon\|_{H^2(\Omega')} \\
&\leq C\left(\|v\|_{L^2(\Omega')} + \|f\|_{L^2(\Omega)}\right)\|\sigma + i\omega\varepsilon\|_{H^2(\Omega')}.
\end{aligned}$$

Here, Schwartz inequality was used for the second inequality; Sobolev embedding for the third inequality; and the last inequality comes from (2.6). Hence, the right side of (2.7) is in $L^p(\Omega)$. Now, we apply the standard $W^{2,p}$-estimate for Poisson's equation (2.7) to get

$$\|v\|_{W^{2,p}(\Omega')} \leq C\left(\|v\|_{L^p(\Omega)^2} + \|f\|_{L^p(\Omega)}\right). \quad \square$$

3. Sets of proper boundary conditions

The main purpose of this section is to choose "good" boundary datum φ in (1.1) so that the measurements of the corresponding vector potential u_ω are helpful in our reconstruction algorithm. Such a set of good functions, henceforth coined as *a set of proper boundary conditions*, is defined as follows.

Definition 3.1. Let $\varphi \in H^{1/2}(\partial\Omega)^2$. We say that φ is a proper set of boundary conditions if and only if the 2×2 matrix ∇u_σ is invertible in Ω for all $\sigma \in \sigma_0 + \mathcal{S}$ where the vector u_σ denotes the solution of the boundary value problem

$$\begin{cases} \nabla \cdot \sigma \nabla u = 0 & \text{in } \Omega, \\ u = \varphi & \text{on } \partial\Omega. \end{cases}$$

The existence of a set of proper boundary conditions was proved in [6,19,47].

The following proposition is the main result of this section.

Proposition 3.1. *For all $(\sigma, \varepsilon) \in \widetilde{\mathcal{S}}$, we denote by u_ω the solution of (1.1) with φ being a proper set of boundary conditions. There exist $N > 1$ open pairwise disjoint open subsets $B_1, B_2, \cdots, B_N$ of Ω, and N frequencies $\omega_1, \cdots, \omega_N \in (\underline{\omega}, \overline{\omega})$ such that*

(i) $\overline{\Omega'} \subset \cup_{j=1}^N \overline{B}_j \subset \Omega$;
(ii) The matrix $A_{\omega_j}(x) = \nabla u_{\omega_j}$ is invertible for all $x \in B_j$.

In [1], G. Alberti has proved the result when the dependence of coefficients on the frequency is different from that in our context. The key of his arguments is the fact that u_ω is analytic with respect to ω. Fortunately, his technique is still applicable to (1.1). We present the proof here for the completeness' sake.

Lemma 3.1. *Let $\mathcal{O}$ be defined by (2.2). The map*

$$\begin{aligned} L : \mathcal{O} &\to H^2_{\mathrm{loc}}(\Omega)^2, \\ \omega &\mapsto \quad u_\omega, \end{aligned}$$

where u_ω is the solution to (1.1), is analytic. Moreover, the derivative of L at ω_0 is given by the solution of

$$\begin{cases} \nabla \cdot (\sigma + i\omega_0\varepsilon)\nabla w = -\nabla \cdot i\varepsilon\nabla L(\omega_0) & \text{in } \Omega, \\ w = 0 & \text{on } \partial\Omega \end{cases} \tag{3.1}$$

for all $\omega_0 \in \mathcal{O}$.

Proof. The quotient

$$z := \frac{L(\omega) - L(\omega_0)}{\omega - \omega_0}$$

solves

$$\begin{cases} \nabla \cdot (\sigma + i\omega\varepsilon)\nabla z = -i\nabla \cdot \varepsilon\nabla L(\omega_0) & \text{in } \Omega, \\ z = 0 & \text{on } \partial\Omega. \end{cases} \tag{3.2}$$

Since $\nabla \cdot \varepsilon\nabla L(\omega_0) = 0$ in $\Omega \setminus \overline{\Omega'}$ and $\nabla \cdot \varepsilon\nabla L(\omega_0)$ is in $L^2(\Omega')$ (see Lemma 2.1), we can use Lemma 2.1 again to get

$$\|z\|_{H^2(\Omega)} \leq C\|L(\omega_0)\|_{H^2(\Omega)} \tag{3.3}$$

for some positive constant C.

On the other hand, the difference between z and w satisfies

$$\begin{cases} \nabla \cdot (\sigma + i\omega_0\varepsilon)\nabla(z - w) = -\nabla \cdot i(\omega - \omega_0)\varepsilon\nabla z & \text{in } \Omega, \\ z - w = 0 & \text{on } \partial\Omega, \end{cases} \tag{3.4}$$

where w is defined by (3.1). Applying Lemma 2.1 one more time allows us to obtain

$$\|z - w\|_{H^2(\Omega)} \leq C|\omega - \omega_0|\|\nabla z\|_{H^2(\Omega)}.$$

This, together with (3.3), completes the proof of this lemma. □

We are now in position to prove Proposition 3.1.

Proof of Proposition 3.1. Let $\Omega'' = \{x \in \Omega \ : \ \mathrm{dist}(x, \partial\Omega) > c_0/2\}$, so that $\Omega' \subset\subset \Omega'' \subset\subset \Omega$. From Lemma 2.1, $u_\omega \in W^{2,p}(\Omega'')$ for any $p > 2$. Hence, it follows from Sobolev embedding that $u_\omega \in \mathcal{C}^{1,\alpha}(\overline{\Omega''})$ for some $\alpha \in (0, 1)$. Thus we can consider u_ω and ∇u_ω pointwisely. We employ the ideas in [1] to prove the proposition. Since $\det : \mathcal{C}(\overline{\Omega''})^{2\times 2} \to \mathcal{C}(\overline{\Omega''})$ is multilinear and bounded and

$$\begin{aligned} \mathcal{O} &\to \mathcal{C}^{1,\alpha}(\overline{\Omega''})^2 \\ \omega &\mapsto u_\omega \end{aligned}$$

is analytic thanks to Lemma 3.1. Moreover,

$$\begin{aligned}\mathcal{O} &\to \mathcal{C}^{0,\alpha}(\overline{\Omega''})\\ \omega &\mapsto \det(\nabla u_\omega)\end{aligned}$$

is also analytic. For $x \in \Omega$, if $\det A_\omega(x) = 0$ for every $\omega \in [\underline{\omega}, \overline{\omega}]$ then for all $\omega \in \mathcal{O}$, $\det A_\omega(x) = 0$ by the analytic continuation theorem. In particular, $\det A_0(x) = 0$ which conflicts with the choice of proper boundary conditions. Hence, we can find $\omega_x \in (\underline{\omega}, \overline{\omega})$ such that $|\det A_{\omega_x}(x)| > 0$. Moreover, since the map $|\det A_{\omega_x}(\cdot)|$ is continuous, it is strictly positive in the ball $B_{r_x}(x)$, centered at x and of radius $r_x > 0$. Noting that $\cup_{x\in\Omega'} B_{r_x}(x)$ covers Ω', we can use the compactness of $\overline{\Omega'}$ in $\mathbb{R}^2$ to complete the proof. □

From now on, a proper set of boundary conditions φ has been chosen. However, in practice, one might not know the values of frequencies and the set $B_1, \cdots, B_N$. We thus suggest to measure the data u_ω for all $\omega \in (\underline{\omega}, \overline{\omega})$. The following corollary of Proposition 3.1 will be useful for the sequel.

Corollary 3.1. *If φ is a proper set of boundary conditions then we can find $\lambda > 0$ such that*

$$\int_{\underline{\omega}}^{\overline{\omega}} |\det \nabla u_\omega(x)| dx > \lambda,$$

where $u_\omega(x)$ is the solution of (1.1).

It is worth mentioning that using the techniques of [2] it is possible to choose only a finite number of frequencies in the interval instead of an infinite number. By [5], if the coefficients are analytic then it is expected that the number of needed frequencies is three.

4. The reconstruction method

4.1. Optimization scheme

Let the function $U_\omega = F[\sigma_*, \varepsilon_*; \omega]$ represent the measurement of the solution vector with σ_* and ε_* being the true distributions.

Consider

$$\begin{aligned}F : \widetilde{\mathcal{S}} \times (\underline{\omega}, \overline{\omega}) &\to H^2(\Omega)^2\\ (\sigma, \varepsilon; \omega) &\mapsto u_\omega - U_\omega,\end{aligned}$$

where again u_ω is the solution to (1.1) with a proper set of boundary conditions φ. Here $\widetilde{\mathcal{S}}$ is considered as a subset of the Hilbert space $H^2(\Omega)^2$. Note that F is well-defined thanks to Lemma 2.1.

To reconstruct σ and ε, we minimize the discrepancy functional

$$J[\sigma, \varepsilon] = \frac{1}{2} \int_{\underline{\omega}}^{\overline{\omega}} \|F[\sigma, \varepsilon; \omega]\|^2_{H^1(\Omega)} d\omega$$

for $(\sigma, \varepsilon) \in \widetilde{\mathcal{S}}$.

We first investigate the differentiability of F with respect to the pair of admittivity (σ, ε). For doing so, we need one more notation. Let $A : B = \sum_{i,j} a_{ij} b_{ij}$ for two matrices $A = (a_{ij})$ and $B = (b_{ij})$. Let $\langle\, , \rangle_{H^s}$ denote the $H^s(\Omega)^2$-scalar product for $s = 1, 2$. The following lemma holds.

Lemma 4.1.

(i) *The map F is Fréchet differentiable in $(\sigma,\varepsilon)\in\widetilde{\mathcal{S}}$. For all $(h,k)\in\mathcal{S}$, $DF[\sigma,\varepsilon;\omega](h,k)$ is given by the solution of*

$$\begin{cases} \nabla\cdot(\sigma+i\omega\varepsilon)\nabla v_\omega = -\nabla\cdot(h+i\omega k)\nabla u_\omega & \text{in } \Omega,\\ v_\omega = 0 & \text{on } \partial\Omega. \end{cases} \tag{4.1}$$

Moreover, DF is Lipschitz continuous with respect to (σ,ε).

(ii) *J is Fréchet differentiable in $(\sigma,\varepsilon)\in\widetilde{\mathcal{S}}$. Moreover, for all $(h,k)\in\mathcal{S}$,*

$$\begin{aligned} DJ[\sigma,\varepsilon](h,k) &= \Re e\int_{\underline{\omega}}^{\overline{\omega}} \langle DF[\sigma,\varepsilon;\omega](h,k), F[\sigma,\varepsilon;\omega]\rangle_{H^1}\\ &= \Re e\int_{\underline{\omega}}^{\overline{\omega}} \langle (h,k), DF[\sigma,\varepsilon;\omega]^*(F[\sigma,\varepsilon;\omega])\rangle_{H^2}, \end{aligned} \tag{4.2}$$

where $DF[\sigma,\varepsilon;\omega]^*$ is the adjoint of $DF[\sigma,\varepsilon;\omega]$.

(iii) *Furthermore, for all $(h,k)\in\mathcal{S}$,*

$$DJ[\sigma,\varepsilon](h,k) = \Re e\int_{\underline{\omega}}^{\overline{\omega}}\int_{\Omega}(h+i\omega k)\nabla u_\omega : \nabla p_\omega\, d\omega, \tag{4.3}$$

where $p_\omega\in H^2(\Omega)$ is the solution to the adjoint problem

$$\begin{cases} \nabla\cdot(\sigma+i\omega\varepsilon)\nabla p_\omega = \overline{F(\sigma,\varepsilon;\omega)} - \Delta\overline{F(\sigma,\varepsilon;\omega)} & \text{in } \Omega,\\ p_\omega = 0 & \text{on } \partial\Omega. \end{cases} \tag{4.4}$$

Proof. Take $(h,k)\in\mathcal{S}$ such that $(\sigma+h,\varepsilon+k)$ still belongs to $\widetilde{\mathcal{S}}$. Define

$$w_{h,k} = F[\sigma+h,\varepsilon+k;\omega] - F[\sigma,\varepsilon;\omega]\in H_0^1(\Omega)^2.$$

We have

$$\begin{aligned} \nabla\cdot(\sigma+h+i\omega(\varepsilon+k))\nabla w_{h,k} &= -\nabla\cdot(\sigma+h+i\omega(\varepsilon+k))\nabla(F[\sigma,\varepsilon;\omega]+U_\omega)\\ &= \nabla\cdot(h+i\omega k)\nabla(F[\omega,\sigma,\varepsilon]+U_\omega). \end{aligned}$$

Using Sobolev embedding and Lemma 2.1, we have

$$\begin{aligned} \|w_{h,k}\|_{H^2(\Omega)^2} &\le C\|\nabla\cdot(h+i\omega k)\nabla(F[\sigma,\varepsilon;\omega]+U_\omega)\|_{L^2(\Omega')^2}\\ &\le C\Big(\|h+i\omega k\|_{L^\infty(\Omega')}\|F[\sigma,\varepsilon;\omega]+U_\omega\|_{H^2(\Omega')^2}\\ &\qquad + \|\nabla(h+i\omega k)\|_{L^4(\Omega')^2}\|\nabla(F[\sigma,\varepsilon;\omega]+U_\omega)\|_{L^4(\Omega')^{2\times 2}}\Big)\\ &\le C\left(\|h\|_{H^2(\Omega)}+\|k\|_{H^2(\Omega)}\right)\left(\|F[\omega,\sigma,\varepsilon]\|_{H^2(\Omega')^2}+\|U_\omega\|_{H^2(\Omega')^2}\right). \end{aligned} \tag{4.5}$$

The function $w_{h,k}-v_\omega\in H_0^1(\Omega)$ and satisfies

$$\nabla\cdot(\sigma+i\omega\varepsilon)\nabla(w_{h,k}-v_\omega) = -\nabla\cdot(h+i\omega k)\nabla w_{h,k}.$$

Thus, again by repeating the estimates as in (4.5), we get

$$\begin{aligned}\|w_{h,k}-v_\omega\|_{H^2(\Omega)^2} &\le C\left(\|h\|_{H^2(\Omega)}+\|k\|_{H^2(\Omega)}\right)\|w_{h,k}\|_{H^2(\Omega')^2}\\ &\le C\left(\|h\|_{H^2(\Omega)}+\|k\|_{H^2(\Omega)}\right)^2\left(\|F[\omega,\sigma,\varepsilon]\|_{H^2(\Omega')^2}+\|U_\omega\|_{H^2(\Omega')^2}\right).\end{aligned}$$

Item (i) has been then proved. Moreover, it is easy to see that DF is Lipschitz continuous with respect to (σ,ε). In fact, let (σ,ε) and (σ',ε') be in $\widetilde{\mathcal{S}}$. Let (h,k) be in $\mathcal{S}$. Then, $DF[\sigma,\varepsilon;\omega](h,k)-DF[\sigma',\varepsilon';\omega](h,k)$ is solution to the following equation:

$$\begin{cases}\nabla\cdot(\sigma+i\omega\varepsilon)\nabla\left(DF[\sigma,\varepsilon;\omega](h,k)-DF[\sigma',\varepsilon';\omega](h,k)\right)=\\ \quad-\nabla\cdot(h+i\omega k)\nabla(F[\sigma,\varepsilon;\omega]-F[\sigma',\varepsilon';\omega])\\ \quad-\nabla\cdot(\sigma-\sigma'+i\omega(\varepsilon-\varepsilon'))\nabla DF[\sigma',\varepsilon';\omega](h,k)\quad\text{in }\Omega,\\ DF[\sigma,\varepsilon;\omega](h,k)-DF[\sigma',\varepsilon';\omega](h,k)=0\quad\text{on }\partial\Omega.\end{cases}$$

Therefore, applying similar estimate as in (4.5), we have

$$\begin{aligned}&\|(DF[\sigma,\varepsilon;\omega]-DF[\sigma',\varepsilon';\omega])(h,k)\|_{H^2(\Omega)^2}\\ &\quad\le C\left(\|h+i\omega k\|_{H^2(\Omega)}\|F[\sigma,\varepsilon;\omega]-F[\sigma',\varepsilon';\omega])\|_{H^2(\Omega')^2}\right.\\ &\qquad\left.+\|\sigma-\sigma'+i\omega(\varepsilon-\varepsilon')\|_{H^2(\Omega)}\|DF[\sigma',\varepsilon';\omega](h,k)\|_{H^2(\Omega)^2}\right).\end{aligned}\tag{4.6}$$

Since $F[\sigma,\varepsilon;\omega]-F[\sigma',\varepsilon';\omega]$ satisfies

$$\nabla\cdot(\sigma+i\omega\varepsilon)\nabla(F[\sigma,\varepsilon;\omega]-F[\sigma',\varepsilon';\omega])=-\nabla\cdot(\sigma-\sigma'+i\omega(\varepsilon-\varepsilon'))\nabla(F[\sigma',\varepsilon';\omega]+U_\omega),$$

we apply a similar estimate as in (4.5) to get Lipschitz continuity of F:

$$\begin{aligned}\|F[\sigma,\varepsilon;\omega]-F[\sigma',\varepsilon';\omega])\|_{H^2(\Omega')}\le{}& C\|\sigma-\sigma'+i\omega(\varepsilon-\varepsilon')\|_{H^2(\Omega)}\\ &\times\left(\|F[\sigma',\varepsilon';\omega]\|_{H^2(\Omega')^2}+\|U_\omega\|_{H^2(\Omega')^2}\right).\end{aligned}\tag{4.7}$$

Noting that $DF[\sigma,\varepsilon;\omega](h,k)$ is the solution of (4.1), we also have

$$\|DF[\sigma',\varepsilon';\omega](h,k)\|_{H^2(\Omega')}\le C\|h+i\omega k\|_{H^2(\Omega)}\|\left(F[\sigma',\varepsilon';\omega]\|_{H^2(\Omega')^2}+\|U_\omega\|_{H^2(\Omega')^2}\right).\tag{4.8}$$

Hence, combining estimates (4.6)–(4.8), we have

$$\begin{aligned}\|DF[\sigma,\varepsilon;\omega]-DF[\sigma',\varepsilon';\omega]\|_{\mathcal{L}(H^2(\Omega),H^2(\Omega))}\le{}& C\|\sigma-\sigma'+i\omega(\varepsilon-\varepsilon')\|_{H^2(\Omega)}\\ &\times\left(\|F[\sigma',\varepsilon';\omega]\|_{H^2(\Omega')^2}+\|U_\omega\|_{H^2(\Omega')^2}\right).\end{aligned}$$

Item (ii) can be easily proved by using arguments similar to those used above. Item (iii) follows by integration by parts. □

We can now apply the gradient descent method to minimize the discrepancy functional J. We compute the iterates

$$(\sigma_{n+1},\varepsilon_{n+1})=T[\sigma_n,\varepsilon_n]-\mu DJ[T[\sigma_n,\varepsilon_n]],\tag{4.9}$$

where $\mu>0$ is the step size and $T[f]$ is any approximation of the Hilbert projection from $H^2(\Omega)^2$ onto $\overline{\widetilde{\mathcal{S}}}$ with $\overline{\widetilde{\mathcal{S}}}$ being the closure of $\widetilde{\mathcal{S}}$ (in the H^2-norm). The derivative $DJ[T[\sigma_n,\varepsilon_n]]$ is given by

$$DJ[T[\sigma_n,\varepsilon_n]] = (-\Re e\,\nabla u_\omega : \nabla p_\omega, \omega \Im m\,\nabla u_\omega : \nabla p_\omega),$$

where u_ω and p_ω are respectively the solutions to (1.1) and (4.4) with $(\sigma,\varepsilon) = T[\sigma_n,\varepsilon_n]$.

The presence of T is necessary because (σ_n,ε_n) might not be in $\widetilde{\mathcal{S}}$.

Using (iv) we can show that the optimal control algorithm (4.9) is nothing else than the following Landweber scheme [33,28] given by

$$\begin{aligned}&(\sigma_{n+1},\varepsilon_{n+1})\\ &\quad = T[\sigma_n,\varepsilon_n] - \mu \int_{\underline{\omega}}^{\overline{\omega}} DF^*[T[\sigma_n,\varepsilon_n];\omega](F[T[\sigma_n,\varepsilon_n];\omega])\,d\omega.\end{aligned} \tag{4.10}$$

4.2. Initial guess

To initialize the previous optimal control algorithm, we need to construct an initial guess for the electrical property distributions σ and ϵ.

Consider the solution u_ω to (1.1). For all $x \in \Omega$,

$$\Delta u_\omega + \frac{\nabla u_\omega^T \nabla(\sigma + i\omega\varepsilon)}{\sigma + i\omega\varepsilon} = 0.$$

It follows that

$$A_\omega^T \frac{\nabla(\sigma + i\omega\varepsilon)}{\sigma + i\omega\varepsilon} = -\nabla \cdot A_\omega, \tag{4.11}$$

where

$$A_\omega = \nabla u_\omega.$$

Equation (4.11) gives us several ways to reconstruct both σ and ε. We suggest to define the map $\gamma_\omega = \log(\sigma + i\omega\varepsilon)$, whose imaginary part is chosen in $[0, \frac{\pi}{2})$, and solve

$$\begin{cases} \Delta\gamma_\omega = \nabla \cdot (-(\overline{A_\omega} A_\omega^T)^\dagger \overline{A_\omega} \nabla \cdot A_\omega) & \text{in } \Omega,\\ \gamma_\omega = \log(\sigma_0 + i\omega\varepsilon_0) & \text{on } \partial\Omega, \end{cases} \tag{4.12}$$

where $\dagger$ denotes the pseudo-inverse. The knowledge of γ_ω implies those of σ and ε. We denote by σ_I and ε_I the obtained functions by averaging γ_ω over ω:

$$\sigma_I + i\frac{(\overline{\omega}) + \underline{\omega}}{2}\varepsilon_I = \frac{1}{\overline{\omega} - \underline{\omega}} \int_{\underline{\omega}}^{\overline{\omega}} e^{\gamma_\omega} d\omega,$$

where γ_ω is given by (4.12). We use σ_I and ε_I as the initial guess for our desired coefficients.

4.3. Convergence of the minimizing sequence

The following theorem holds.

Theorem 4.1. *For all $(h,k) \in \mathcal{S}$, we have the following estimate:*

$$\int_{\underline{\omega}}^{\overline{\omega}} \|DF[\sigma,\varepsilon;\omega](h,k)\|_{H^1(\Omega)^2} d\omega \geq C\|(h,k)\|_{H^2(\Omega)^2} \tag{4.13}$$

for some positive constant C.

Proof. Assume to the contrary that (4.13) is not true. That means we can find h_n and k_n in $\mathcal{S}$ such that

$$\|h_n\|_{H^2(\Omega)} + \|k_n\|_{H^2(\Omega)} = 1$$

and

$$\int_{\underline{\omega}}^{\overline{\omega}} \|DF[\sigma,\varepsilon;\omega](h_n,k_n)\|_{H^1(\Omega)} d\omega \to 0$$

as $n \to \infty$. By compactness, up to extracting a subsequence, we can assume that

$$(h_n,k_n) \rightharpoonup (h,k) \quad \text{in } H_0^1(\Omega)^2. \tag{4.14}$$

Denote by u_ω the vector $F[\sigma,\varepsilon;\omega]$ and v_ω^n the vector $DF[\sigma,\varepsilon;\omega](h_n,k_n)$. We have

$$v_\omega^n \to 0 \quad \text{in } H_0^1(\Omega)$$

for all $\omega \in (\underline{\omega},\overline{\omega})$.

Recall $N, B_1, \cdots, B_N, \omega_1, \cdots, \omega_N$, as in Proposition 3.1. Fixing $j \in \{1,\cdots,N\}$, we have

$$\begin{aligned} -\nabla\cdot(\sigma+i\omega_j\varepsilon)\nabla v_{\omega_j}^n &= \nabla\cdot(h_n+i\omega_j k_n)\nabla u_{\omega_j} \\ &= (\sigma+i\omega_j\varepsilon)\nabla u_{\omega_j}^T \nabla \frac{h_n+i\omega_j k_n}{\sigma+i\omega_j\varepsilon} \end{aligned}$$

in B_j. Equivalently,

$$\nabla u_{\omega_j}^T \nabla \frac{h_n+i\omega_j k_n}{\sigma+i\omega_j\varepsilon} = -\nabla\log(\sigma+i\omega_j\varepsilon)\cdot\nabla v_{\omega_j}^n - \Delta v_{\omega_j}^n.$$

Note that the left-hand side of the equation above tends to 0 in $H^{-1}(\Omega)$, so is $\nabla\frac{h_n+i\omega_j k_n}{\sigma+i\omega_j\varepsilon}$ in $L^2(B_j)$. By using Poincaré's inequality and the fact that $\overline{\Omega'} \subset \cup_{j=1}^N \overline{B}_j$, we arrive at $h = k = 0$. Since $(h_n,k_n) \in \mathcal{S}$, $\|h_n\|_{H^2(\Omega)} + \|k_n\|_{H^2(\Omega)} \to 0$, which contradicts the assumption. □

Note that as a direct consequence of Theorem 4.1, it follows that

$$\left(\int_{\underline{\omega}}^{\overline{\omega}} \|DF[\sigma,\varepsilon;\omega](h,k)\|_{H^1(\Omega)^2}^2 d\omega\right)^{\frac{1}{2}} \geq C\|(h,k)\|_{H^2(\Omega)^2} \tag{4.15}$$

for some positive constant C. Hence, Theorem 4.1 and Proposition A.1 yield our main result in this paper.

Theorem 4.2. *The sequence defined in (4.10) converges to the true admittivity $(\sigma_*, \varepsilon_*)$ of Ω in the following sense: there is $\eta > 0$ such that if $\|T[\sigma_I, \varepsilon_I] - (\sigma_*, \varepsilon_*)\|_{H^2(\Omega)^2} < \eta$, then*

$$\lim_{n\to+\infty} \|\varepsilon_n - \varepsilon_*\|_{H^2(\Omega)} + \|\sigma_n - \sigma_*\|_{H^2(\Omega)} = 0.$$

5. Numerical illustrations

In this section we present some numerical results to illustrate the performance of the proposed optimal control algorithm for admittivity imaging from micro-electrical data (see Figs. 5.1–5.10).

We consider three regions in the unit square with respective conductivity $2, 3$, and 4. The admittivity of the background medium is $1 + i3\omega$. We produce virtual internal data through the forward problem with the true admittivities. We choose two illuminations $x + ix$, $y + iy$, and calculate the associated potentials u_1 and u_2 in the whole medium with a finite element code. u_1 and u_2 become our measurements for the imaging problem. We first refine the uniform mesh according to the gradient of u_1 and u_2. The initial guess is computed through solving the partial differential equation given in subsection 4.2. It is worth noticing that the reconstruction of an initial guess using (4.12) is always possible. Moreover, in order to make the procedure more robust to noise, one may filter out the smallest eigenvalues of the matrix $\overline{A_\omega} A_\omega^T$.

We observe that in the initial guess the (guessed) permittivities inside the inclusions are different from each other. The reconstruction scheme of the initial guess couples the distributions of the conductivities

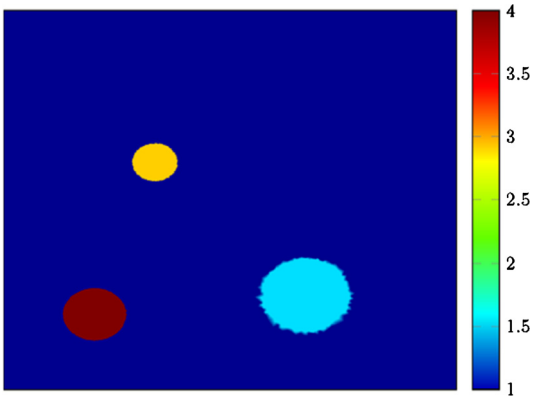

Fig. 5.1. True conductivity σ_*.

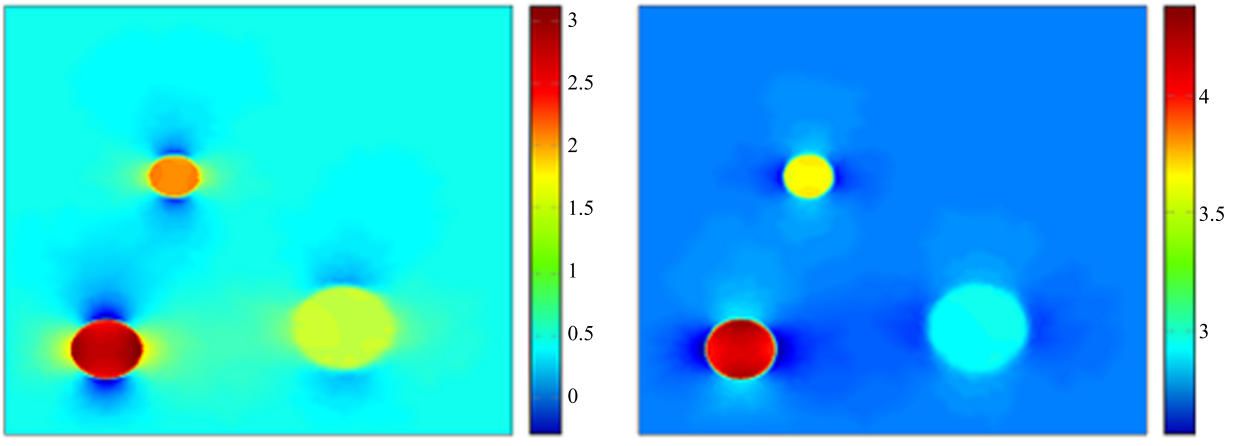

Fig. 5.2. Initial guess of the conductivity (on the left) and the permittivity (on the right).

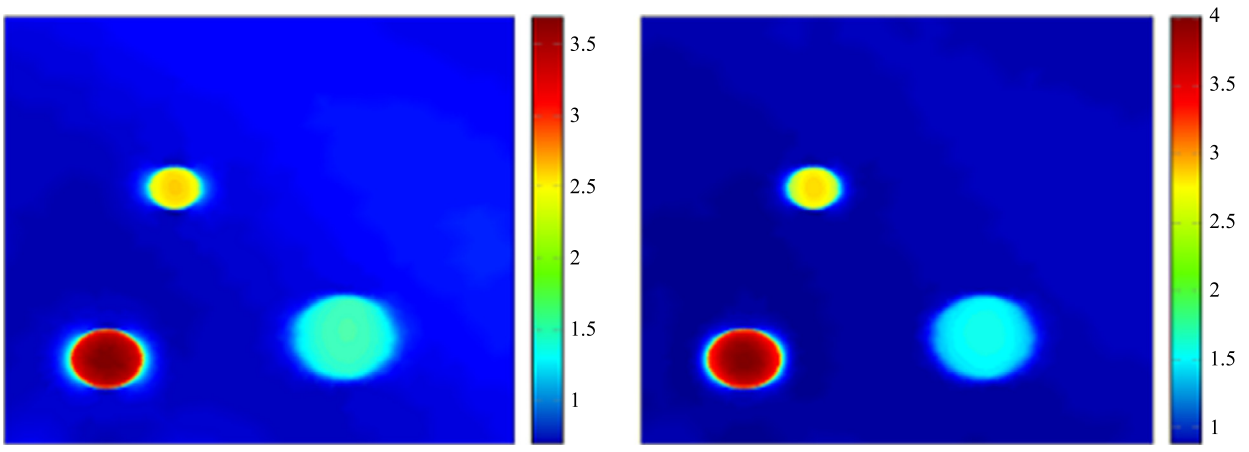

Fig. 5.3. Reconstructed conductivity after 20 (on the left) and 40 (on the right) iterations of the algorithm.

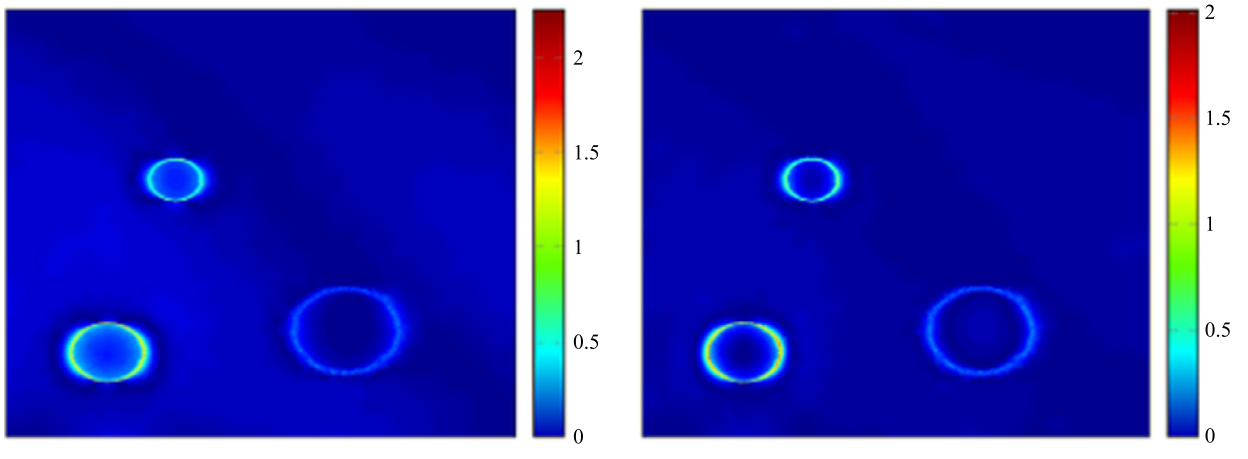

Fig. 5.4. Absolute value of the difference between the reconstructed and true conductivities after 20 (on the left) and 40 (on the right) iterations.

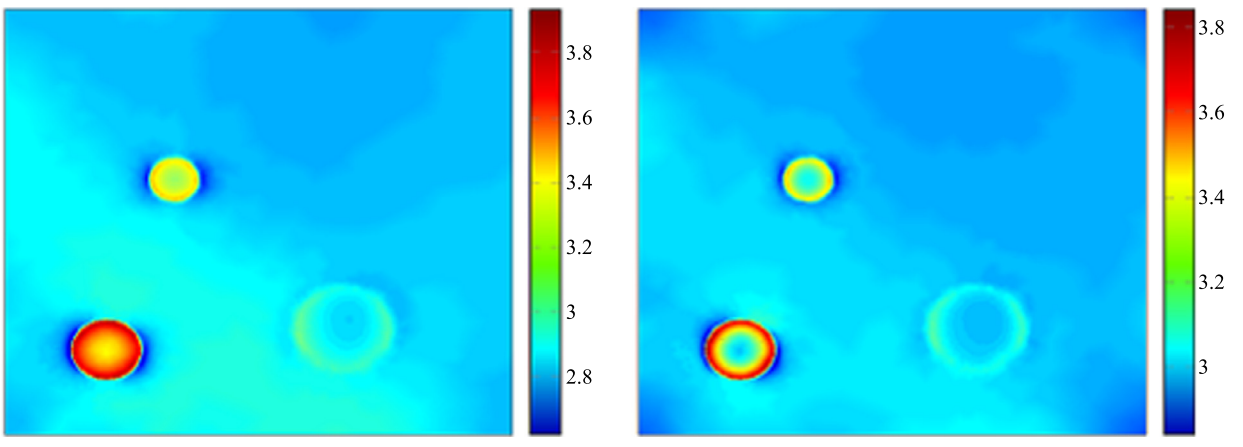

Fig. 5.5. Reconstructed permittivity after 20 (on the left) and 40 (on the right) iterations of the algorithm.

with those of the permittivities. We note that the mesh used for simulating the data is not the same as for the reconstruction of the conductivity and permittivity distributions.

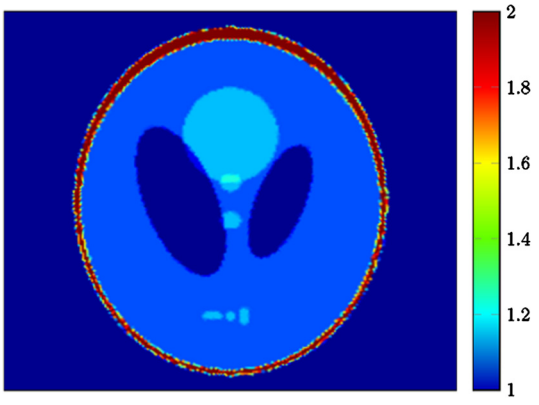

Fig. 5.6. True conductivity σ_*.

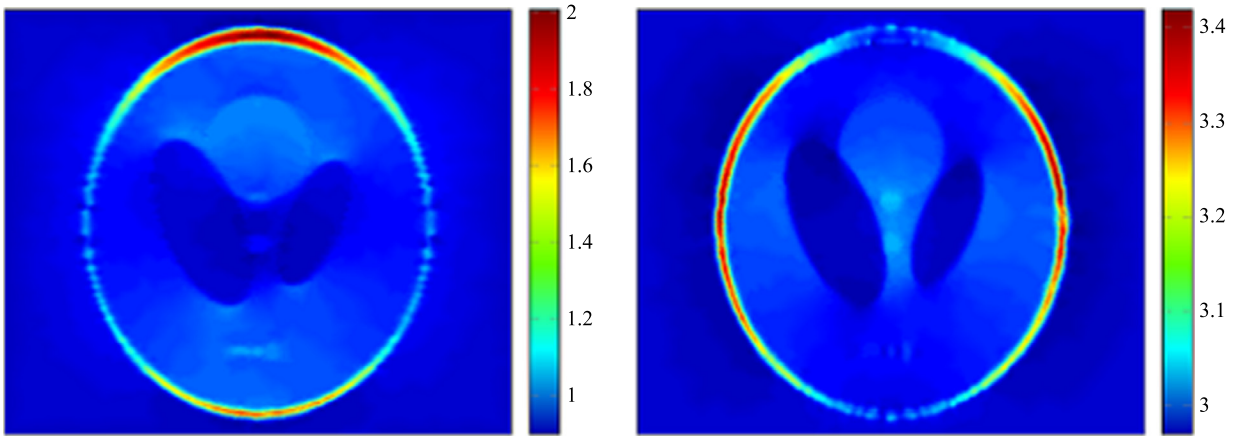

Fig. 5.7. Initial guess of the conductivity (on the left) and the permittivity (on the right).

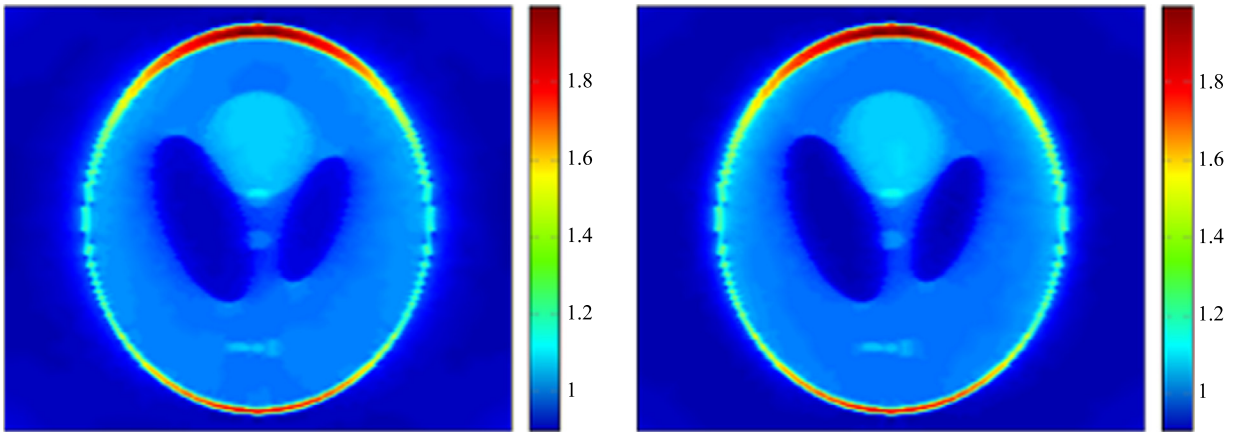

Fig. 5.8. Reconstructed conductivity after 20 (on the left) and 40 (on the right) iterations of the algorithm.

It is also worth emphasizing that in our case the matrix data is invertible everywhere in the domain and therefore, there is no need in this case for taking multi-frequency measurements.

The results of the reconstructions are presented after 20 and 40 iterations. The difference between the true and reconstructed conductivities are shown. After 20 iterations, the shapes of the inclusions are well

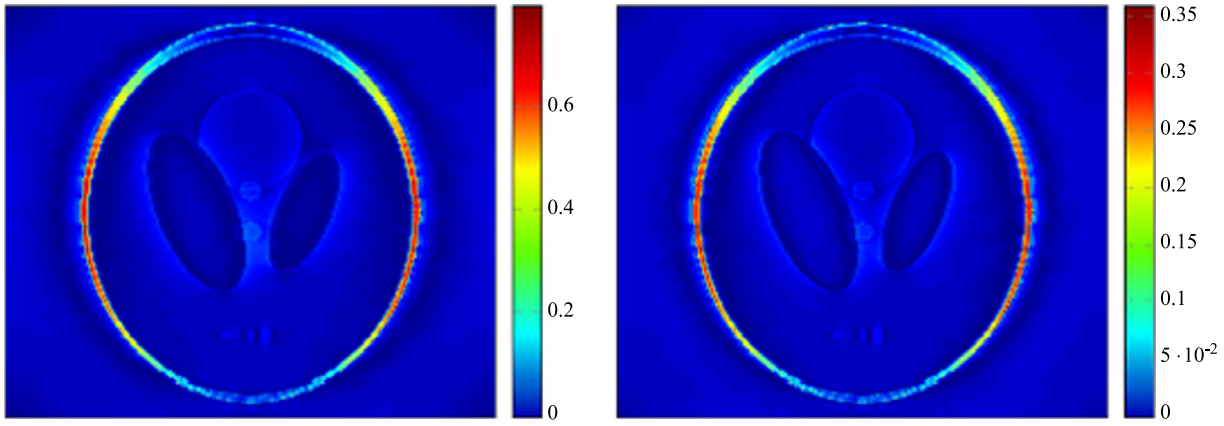

Fig. 5.9. Absolute value of the difference between the reconstructed and true conductivities after 20 (on the left) and 40 (on the right) iterations.

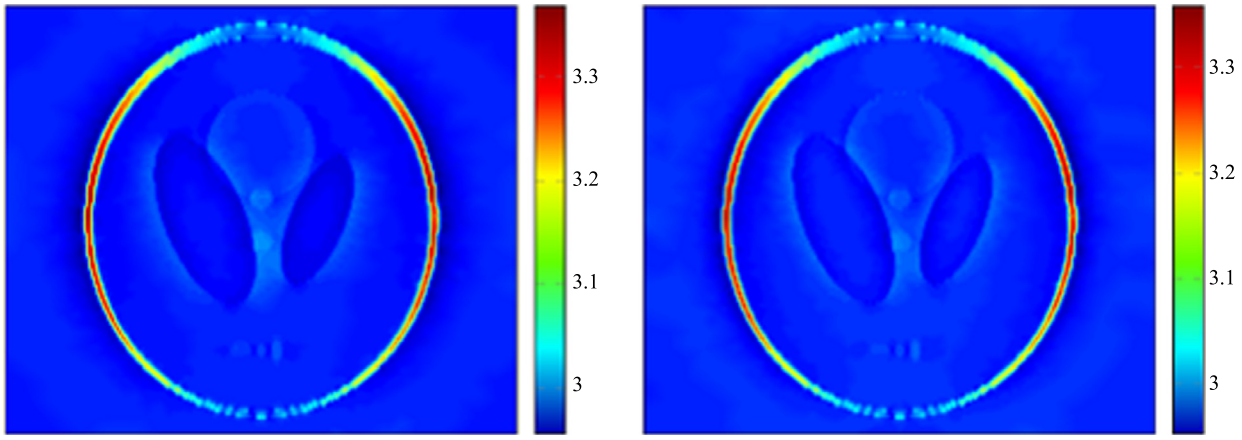

Fig. 5.10. Reconstructed permittivity after 20 (on the left) and 40 (on the right) iterations of the algorithm.

reconstructed however the values of the conductivity inside are still not correct. 40 iterations are enough to well reconstruct both the shapes, the conductivities, and the permittivities.

In the second set of numerical examples, we consider a different phantom. The conductivities are between 1 and 2 as shown below while the permittivity is constant and equal to 3 everywhere. Again, after 40 iterations starting from the initial guess given in subsection 4.2, the reconstructed images are well resolved.

6. Concluding remarks

In this paper we have proposed for the first time an optimal control algorithm for admittivity imaging from multi-frequency micro-electrical data. We have proved its convergence and its local stability. Our approach in this paper can be extended to elastography and can be used to image both shear modulus and viscosity tissue properties from internal displacement measurements. More generally, it opens a door for convergence analysis for optimal control type approaches in hybrid imaging, where two waves are combined in order to enhance resolution and stability [9]. Another interesting problem is to image tissues with anisotropic impedance distribution from micro-electrical data. This would be the subject of a forthcoming paper. Finally, as the numerical results tend to show, it would be very interesting to find the number (possibly one) of needed frequencies in order to insure convergence of the optimal control approach.

Acknowledgments

The authors are very grateful to G.S. Alberti for interesting and illuminating discussions.

Appendix A. The convergence of the Landweber sequence with a Hilbert projection

This appendix follows from [28]; see also [29]. It proves the convergence of the Landweber scheme with a Hilbert projection.

Let X and Y be Hilbert spaces and $F : K \times (\underline{\omega}, \overline{\omega}) \to Y$ be a differentiable map where K is a convex subset of X. Let $\langle\,,\,\rangle_X$ and $\langle\,,\,\rangle_Y$ denote the scalar products in X and Y, respectively.

We are interested in solving the equation

$$F[x_*;\omega] = 0 \quad \text{for all } \omega \in (\underline{\omega}, \overline{\omega}). \tag{A.1}$$

It is natural to minimize

$$J[x] = \frac{1}{2}\int_{\underline{\omega}}^{\overline{\omega}} \|F[x;\omega]\|_Y^2 d\omega, \tag{A.2}$$

with $x \in K$. Assume that $F[\cdot;\omega]$ is Fréchet differentiable. So is J. The derivative of J is given by

$$\begin{aligned} DJ[x](h) &= \int_{\underline{\omega}}^{\overline{\omega}} \langle DF[x;\omega](h), F[x;\omega]\rangle_Y d\omega \\ &= \int_{\underline{\omega}}^{\overline{\omega}} \langle h, DF[x;\omega]^*(F[x;\omega])\rangle_X d\omega, \end{aligned}$$

where the superscript * indicates the dual map. The iteration sequence due to the descent gradient method is given by

$$x_{n+1} = T[x_n] - \mu \int_{\underline{\omega}}^{\overline{\omega}} DF[T[x_n];\omega]^*(F[T[x_n];\omega])\, d\omega. \tag{A.3}$$

Here, μ is a small number and $T[x] \in K$ is an approximation of the Hilbert projection of X onto $\overline{K}$

$$P : X \ni x \mapsto \operatorname{argmin}\{\|x - a\| : a \in \overline{K}\}. \tag{A.4}$$

Without loss of generality, we can assume that

$$\|T[x_n] - P[x_n]\|_X \le 2^{-n}, \quad n \ge 1.$$

The presence of T in (A.3) is necessary because x_n might not be in K and $F[x_n]$ might not be well-defined. The map T above also increases the rate of convergence of (x_n) to x_* due to

$$\|T[x_n] - x_*\|_X \le \|x_n - x_*\|_X + 2^{-n}, \quad n \ge 1. \tag{A.5}$$

The following proposition holds.

Proposition A.1. *Assume that $DF[x;\omega]$ is Lipschitz continuous and that, for all $x, h \in K$,*

$$\int_{\underline{\omega}}^{\overline{\omega}} \|DF[x;\omega](h)\|_Y^2 d\omega \geq c\|h\|_X^2. \tag{A.6}$$

Then the sequence defined in (A.3) converges to x_* provided that x_0 is a "good" initial guess for x_* and μ is sufficiently small.

Proof. Since $DF[x;\omega]$ is Lipschitz continuous, for all x such that $\|x - x_*\|_X < \eta$ with η being a small positive number, we have

$$\begin{aligned}
&\int_{\underline{\omega}}^{\overline{\omega}} \|F[x;\omega] - F[x_*;\omega] - DF[x;\omega](x - x_*)\|_Y^2 d\omega \\
&\qquad \leq C\eta^2 \|x - x_*\|_X^2 \\
&\qquad \leq C\eta^2 \int_{\underline{\omega}}^{\overline{\omega}} \|F[x;\omega] - F[x_*;\omega]\|_Y^2 d\omega
\end{aligned} \tag{A.7}$$

for some positive constant C. Note that we have used here (A.6) and the mean-value theorem for the second inequality above.

For all $n \geq 1$, let

$$\epsilon_n[\omega] = F[T[x_n];\omega].$$

We have

$$\begin{aligned}
&\|x_{n+1} - x_*\|_X^2 - \|x_n - x_*\|_X^2 - 2^{-n} \\
&\quad \leq \|x_{n+1} - x_*\|_X^2 - \|T[x_n] - x_*\|_X^2 \\
&\quad = 2\langle x_{n+1} - T[x_n], T[x_n] - x_*\rangle_X + \|x_{n+1} - T[x_n]\|_X^2 \\
&\quad \leq 2\mu \int_{\underline{\omega}}^{\overline{\omega}} \langle -DF[T[x_n];\omega]^* \epsilon_n[\omega], T[x_n] - x_*\rangle_X d\omega \\
&\qquad + \int_{\underline{\omega}}^{\overline{\omega}} \langle \mu\epsilon_n[\omega], \mu DF[T[x_n];\omega] DF[T[x_n];\omega]^* (\epsilon_n[\omega])\rangle_Y d\omega \\
&\quad = \int_{\underline{\omega}}^{\overline{\omega}} \langle \epsilon_n[\omega], 2\mu\epsilon_n[\omega] - 2\mu DF[T[x_n];\omega](T[x_n] - x_*)\rangle_Y d\omega - \mu \int_{\underline{\omega}}^{\overline{\omega}} \|\epsilon_n[\omega]\|_Y^2 d\omega \\
&\qquad + \int_{\underline{\omega}}^{\overline{\omega}} \langle \sqrt{\mu}\epsilon_n[\omega], (-I + \mu DF[T[x_n];\omega] DF[T[x_n];\omega]^*)(\sqrt{\mu}\epsilon_n[\omega])\rangle_Y d\omega \\
&\quad \leq 2\mu \left(\int_{\underline{\omega}}^{\overline{\omega}} \|\epsilon_n[\omega]\|_Y^2 d\omega \right)^{\frac{1}{2}} \left(\int_{\underline{\omega}}^{\overline{\omega}} \|\epsilon_n[\omega] - DF[T[x_n];\omega](T[x_n] - x_*)\|_Y^2 d\omega \right)^{\frac{1}{2}}
\end{aligned}$$

$$-\mu\int_{\underline{\omega}}^{\overline{\omega}}\|\epsilon_n[\omega]\|_Y^2 d\omega+\int_{\underline{\omega}}^{\overline{\omega}}\langle\sqrt{\mu}\epsilon_n[\omega],(-I+\mu DF[T[x_n];\omega]DF[T[x_n];\omega]^*))(\sqrt{\mu}\epsilon_n[\omega])\rangle_Y d\omega$$

$$\leq\mu(2\sqrt{C}\eta-1)\int_{\underline{\omega}}^{\overline{\omega}}\|\epsilon_n[\omega]\|_Y^2 d\omega.$$

Here, we have used (A.7) for the last inequality. It follows that

$$\|x_{n+1}-x_*\|_X^2+\mu(1-2\sqrt{C}\eta)\int_{\underline{\omega}}^{\overline{\omega}}\|\epsilon_n\|_Y^2 d\omega-2^{-n}\leq\|x_n-x_*\|_X^2,$$

and therefore,

$$\sum_{n=1}^{\infty}\int_{\underline{\omega}}^{\overline{\omega}}\|F[T[x_n];\omega]\|_Y^2 d\omega\leq\frac{\|x_0-x_*\|_X^2}{\mu(1-2\sqrt{C}\eta)}+1.$$

We now obtain the convergence of (x_n) to x_* using again the mean-value theorem and condition (A.6):

$$c\|T[x_n]-x_*\|_X^2\leq\int_{\underline{\omega}}^{\overline{\omega}}\|DF[\tilde{x}_n;\omega](T[x_n]-x_*)\|_Y^2 d\omega=\int_{\underline{\omega}}^{\overline{\omega}}\|F[T[x_n];\omega]-F[x_*;\omega]\|_Y^2 d\omega\to 0$$

for some $\tilde{x}_n=tT[x_n]+(1-t)x_*$, $t\in(0,1)$. □

References

[1] G.S. Alberti, On multiple frequency power density measurements, Inverse Probl. 29 (2013) 115007.
[2] G.S. Alberti, Enforcing local non-zero constraints in PDEs and applications to hybrid imaging problems, Comm. Partial Differential Equations 40 (2015) 1855–1883.
[3] S.G. Alberti, Absence of critical points of solutions to the Helmholtz equation in 3D, Arch. Ration. Mech. Anal. 222 (2) (2016) 879–894, http://dx.doi.org/10.1007/s00205-016-1013-z.
[4] G.S. Alberti, H. Ammari, K. Ruan, Multi-frequency acousto-electromagnetic tomography, in: A Panorama of Mathematics: Pure and Applied, in: Contemp. Math., vol. 658, 2016, pp. 67–79.
[5] G.S. Alberti, Y. Capdeboscq, On Local non-zero constraints in PDE with analytic coefficients, in: Imaging, Multi-scale and High Contrast Partial Differential Equations, in: Contemp. Math., vol. 660, 2016, pp. 89–97.
[6] G. Alessandrini, R. Magnanini, The index of isolated critical points and solutions of elliptic equations in the plane, Ann. Sc. Norm. Super. Pisa Cl. Sci. 19 (1992) 567–589.
[7] G. Alessandrini, V. Nesi, Univalent σ-harmonic mappings, Arch. Ration. Mech. Anal. 158 (2001) 155–171.
[8] G. Alessandrini, V. Nesi, Quantitative estimates on Jacobians for hybrid inverse problems, in: Bulletin of the South Ural State University, Math. Model. Program. Comput. Softw. 8 (2015) 25–41.
[9] H. Ammari, An Introduction to Mathematics of Emerging Biomedical Imaging, Mathematics and Applications, vol. 62, Springer-Verlag, Berlin, 2008.
[10] H. Ammari, E. Bonnetier, Y. Capdeboscq, M. Tanter, M. Fink, Electrical impedance tomography by elastic deformation, SIAM J. Appl. Math. 68 (2008) 1557–1573.
[11] H. Ammari, Y. Capdeboscq, F. de Gournay, A. Rozanova, F. Triki, Microwave imaging by elastic perturbation, SIAM J. Appl. Math. 71 (2011) 2112–2130.
[12] H. Ammari, Y. Capdeboscq, H. Kang, A. Kozhemyak, Mathematical models and reconstruction methods in magneto-acoustic imaging, European J. Appl. Math. 20 (2009) 303–317.
[13] H. Ammari, J. Garnier, L. Giovangigli, W. Jing, J.K. Seo, Spectroscopic imaging of a dilute cell suspension, arXiv: 1310.1292.
[14] H. Ammari, J. Garnier, W. Jing, Resolution and stability analysis in acousto-electric imaging, Inverse Probl. 28 (2012) 084005.
[15] H. Ammari, J. Garnier, W. Jing, L.H. Nguyen, Quantitative thermo-acoustic imaging: an exact reconstruction formula, J. Differential Equations 254 (2013) 1375–1395.
[16] H. Ammari, J. Garnier, L.H. Nguyen, L. Seppecher, Reconstruction of a piecewise smooth absorption coefficient by an acousto-optic process, Comm. Partial Differential Equations 38 (2013) 1737–1762.

[17] H. Ammari, P. Grasland-Mongrain, P. Millien, L. Seppecher, J.K. Seo, A mathematical and numerical framework for ultrasonically-induced Lorentz force electrical impedance tomography, arXiv:1401.2337.
[18] A. Angersbach, V. Heinz, D. Knorr, Effects of pulsed electric fields on cell membranes in real food systems, Innov. Food Sci. Emerg. Technol. 1 (2000) 135–149.
[19] P. Bauman, A. Marini, V. Nesi, Univalent solutions of an elliptic system of partial differential equations arising in homogenization, Indiana Univ. Math. J. 128 (2000) 53–64.
[20] H. Benjamin, S. Bhansali, S.B. Hoath, W.L. Pickens, R. Smallwood, A planar micro-sensor for bio-impedance measurements, Sens. Actuators, B, Chem. 111–112 (2005) 430–435.
[21] M. Briane, G.W. Milton, V. Nesi, Change of sign of the corrector's determinant for homogenization in three-dimensional conductivity, Arch. Ration. Mech. Anal. 173 (2004) 133–150.
[22] Y. Capdeboscq, On a counter-example to quantitative Jacobian bounds, J. École Polytech. Math. 2 (2015) 171–178.
[23] Y.Z. Chen, L.C. Wu, Second Order Elliptic Equations and Elliptic Systems, Translations of Mathematical Monographs, vol. 174, American Mathematical Society, Providence, RI, 1998, translated from the 1991 Chinese original by Bei Hu.
[24] B. Gebauer, O. Scherzer, Impedance-acoustic tomography, SIAM J. Appl. Math. 69 (2008) 565–576.
[25] I. Giaever, C.R. Keese, Micromotion of mammalian cells measure electrically, Proc. Natl. Acad. Sci. USA 88 (1991) 7896–7900.
[26] M. Giaquinta, L. Martinazzi, An Introduction to the Regularity Theory for Elliptic Systems, Harmonic Maps and Minimal Graphs, second edition, Appunti. Scuola Normale Superiore di Pisa (Nuova Serie), vol. 11, Edizioni della Normale, Pisa, 2012.
[27] D. Gilbarg, N.S. Trudinger, Elliptic Partial Differential Equations of Second Order, Springer-Verlag, Berlin, 1977.
[28] M. Hanke, A. Neubauer, O. Scherzer, A convergence analysis of the Landweber iteration for nonlinear ill-posed problems, Numer. Math. 72 (1995) 21–37.
[29] M.V. de Hoop, L. Qiu, O. Scherzer, Local analysis of inverse problems: Hölder stability and iterative reconstruction, Inverse Probl. 28 (2012) 045001.
[30] C.R. Keese, I. Giaevier, A biosensor that monitors cell morphology with electrical fields, IEEE Eng. Med. Biol. 13 (1994) 402–408.
[31] G. Kresin, V. Mazýa, Maximum Principles and Sharp Constants for Solutions of Elliptic and Parabolic Systems, Mathematical Surveys and Monographs, vol. 183, American Mathematical Society, Providence, RI, 2012.
[32] O. Kwon, J. Lee, J. Yoon, Equipotential line method for magnetic resonance electrical impedance tomography, Inverse Probl. 18 (2002) 1089–1100.
[33] L. Landweber, An iteration formula for Fredholm integral equations of the first kind, Amer. J. Math. 73 (1951) 615–624.
[34] E. Lee, J.K. Seo, E.J. Woo, T. Zhang, Mathematical framework for a new microscopic electrical impedance tomography system, Inverse Probl. 27 (2011) 055008.
[35] P. Linderholm, R. Schoch, Ph. Renaud, Microelectrical impedance tomography for biophysical characterization of thin film biomaterials, in: Transducers, 2003, Boston, MA.
[36] C.M. Lo, C.R. Keese, I. Giaever, Monitoring motion of confluent cells in tissue culture, Exp. Cell Res. 204 (1993) 102–109.
[37] C.M. Lo, C.R. Keese, I. Giaever, Impedance analysis of MDCK cells measured by electrical cell-substrate impedance sensing, Biophys. J. 69 (1995) 2800–2807.
[38] M.S. Mannor, S. Zhang, A.J. Link, M.C. McAlpine, Electrical detection of pathogenic bacteria via immobilized antimicrobial peptides, Proc. Natl. Acad. Sci. 107 (2010) 19207–19212.
[39] G.H. Markxa, C.L. Daveyb, The dielectric properties of biological cells at radiofrequencies: applications in biotechnology, Enzyme Microb. Technol. 25 (1999) 161–171.
[40] Ø.G. Martinsen, S. Grimnes, H.P. Schwan, Interface phenomena and dielectric properties of biological tissue, in: Encyclopedia of Surface and Colloid Science, Marcel Dekker Inc., 2002, pp. 2643–2652.
[41] D. Miklavcic, N. Pavselj, F.X. Hart, Electric Properties of Tissues, Wiley Encyclopedia of Biomedical Engineering, 2006.
[42] P. Mitra, I. Giaever, C.R. Keese, Electric measurements can be used to monitor the attachment and spreading of cells in tissue cultures, Biotechniques 11 (1991) 504–511.
[43] Y. Polevaya, I. Ermolina, M. Schlesinger, B.-Z. Ginzburg, Y. Feldman, Time domain dielectric spectroscopy study of human cells II. Normal and malignant white blood cells, Biochim. Biophys. Acta 1419 (1999) 257–271.
[44] A.R.A. Rahman, C.-M. Lo, S. Bhansali, A micro-electrode array biosensor for impedance spectroscopy of human umbilical vein endothelial cells, Sens. Actuators, B 118 (2006) 115–120.
[45] A.R.A. Rahman, J. Register, G. Vuppala, S. Bhansali, Cell culture monitoring by impedance mapping using a multielectrode scanning impedance spectroscopy system (CellMap), Physiol. Meas. 29 (2008) S227.
[46] H.P. Schwan, Mechanism responsible for electrical properties of tissues and cell suspensions, Med. Prog. Technol. 19 (1993) 163–165.
[47] J.K. Seo, A uniqueness result on inverse conductivity problem with two measurements, J. Fourier Anal. Appl. 2 (1996) 515–524.
[48] J.K. Seo, T.K. Bera, H. Kwon, R. Sadleir, Effective admittivity of biological tissues as a coefficient of elliptic PDE, Comput. Math. Methods Med. (2013) 353849.
[49] J.K. Seo, E.J. Woo, Magnetic resonance electrical impedance tomography (MREIT), SIAM Rev. 53 (2011) 40–68.
[50] J.K. Seo, E.J. Woo, Nonlinear Inverse Problems in Imaging, Wiley, 2013.
[51] F. Triki, Uniqueness and stability for the inverse medium problem with internal data, Inverse Probl. 26 (2010) 095014.
[52] J. Wegener, C.R. Keese, I. Giaever, Electric cell-substrate impedance sensing (ECIS) as a noninvasive means to monitor the kinetics of cell spreading to artificial surfaces, Exp. Cell Res. 259 (2000) 158–166.
[53] T. Widlak, O. Scherzer, Hybrid tomography for conductivity imaging, Inverse Probl. 28 (2012) 084008.
[54] L. Yang, Electrical impedance spectroscopy for detection of bacterial cells in suspensions using interdigitated microelectrodes, Talanta 74 (2008) 1621–1629.